

1 **Endocannabinoid-mediated rescue of somatosensory cortex activity, plasticity**
2 **and related behaviors following an early in life concussion.**

3

4 J. BADAUT^{1,2}, L. HIPPAUF¹, M. MALINCONI¹, B.P. NOARBE³, A. OBENAU³, C. J.
5 DUBOIS¹

6 ¹ Univ. Bordeaux, CNRS, CRMSB, UMR 5536, F-33000 Bordeaux, France;

7 ² Department of Basic Sciences, Loma Linda University School of Medicine, Loma Linda, CA,
8 USA;

9 ³ Department of Pediatrics, University of California, Irvine, CA, USA.

10

11

12 Corresponding author:

13 Christophe J. Dubois

14 CRMSB, CNRS UMR 5536, Université de Bordeaux, 146 rue Léo Saignat, 33076 Bordeaux,
15 France.

16 E-mail address: christophe.dubois@u-bordeaux.fr.

17

18 Key words: juvenile concussion, early life brain injury, sensory integration, *in vivo* calcium
19 imaging, long-term jmTBI consequences, endocannabinoid degradation, aging

20 Abstract.

21

22 Due to the assumed plasticity of immature brain, early in life brain alterations are thought to
23 lead to better recoveries in comparison to the mature brain. Despite clinical needs, how
24 neuronal networks and associated behaviors are affected by early in life brain stresses, such
25 as pediatric concussions, have been overlooked. Here we provide first evidence in mice that
26 a single early in life concussion durably increases neuronal activity in the somatosensory
27 cortex into adulthood, disrupting neuronal integration while the animal is performing sensory-
28 related tasks. This represents a previously unappreciated clinically relevant mechanism for
29 the impairment of sensory-related behavior performance. Furthermore, we demonstrate that
30 pharmacological modulation of the endocannabinoid system a year post-concussion is well-
31 suited to rescue neuronal activity and plasticity, and to normalize sensory-related behavioral
32 performance, addressing the fundamental question of whether a treatment is still possible
33 once post-concussive symptoms have developed, a time-window compatible with clinical
34 treatment.

35 Introduction.

36 A conserved evolutionary aspect of all living creatures is the necessity to adapt its behaviors
37 according to changes in the environment. In complex animals, treatment of the sensory
38 inputs that relate to the environment require proper integration and processing of the stimuli
39 to ensure adaptative response and survival. In a number of brain disorders, the central
40 processing of sensory inputs is altered, leading eventually to the overall morbidity of the
41 condition. In human subjects, failure to properly integrate sensory inputs leads to a wide
42 variety of impairments, considerably worsening the patient's quality of life. These alterations
43 can occur at any time during the lifespan, and an often-overlooked question, yet essential to
44 develop *ad hoc* therapeutical strategies, is whether these alterations would lead to the same
45 consequences in the developing brain in comparison to the adult brain. Indeed, because of
46 the on-going plasticity mechanisms in the early times of brain development, it is often
47 assumed that this would compensate for the disturbances¹.

48 While brain injuries can lead to focal disruption of specific brain regions, diffuse injuries,
49 typically seen in concussions, initiate a brain-wide neurometabolic cascade that have the
50 potential to durably disrupt brain functioning. While for concussions recovery will be achieved
51 within days, post- concussion symptoms might perdure months to years, for 10 to 20% of
52 adults^{2,3}. While all age groups are likely to be affected by head concussion, children and
53 adolescents represent a large fraction of emergency admissions for concussions to mild
54 traumatic brain injuries (mTBI), and are more susceptible to developing persistent post-
55 concussive syndromes^{4,5}. Those symptoms include cognitive, psychosocial and physical
56 deficits with a high prevalence in altered sensory integration such that the assessment of
57 balance and postural stability (that are likely the result of central sensory integration
58 dysfunction rather than vestibular or oculomotor alterations⁶) are a means to assess the
59 extent of the impairment and its recovery. Considering this higher susceptibility to early life
60 events, it is confounding that the underlying cellular and molecular mechanisms have been
61 overlooked in juvenile models of concussion, especially in the long-term range. Without that
62 knowledge, specific treatments are currently unavailable in clinical settings.

63 Sensory processing involves various brain regions, with the somatosensory cortex
64 representing a critical hub receiving sensory neuronal inputs. In several adult models of
65 moderate to severe TBI, the neuronal activity of the somatosensory cortex has been shown
66 to be exacerbated acutely following the ipsilateral injury⁷⁻⁹. In those models, neuronal activity
67 of other brain regions has also been shown to be altered⁸⁻¹⁵. Similar consequences were
68 found within weeks following a juvenile moderate to severe TBIs in the somatosensory
69 cortex¹⁶ as well as in the hippocampus¹⁷. While understanding the full time-course of
70 concussion -induced pathology is critical to delineate efficient therapies and despite evidence
71 of the long-term alterations even after mTBI¹⁸, the gap in knowledge of the mid to long term
72 (*i.e.* 3 months or more after injury) functional consequences of TBIs remains to be elucidated
73 with a chronic functional evaluation from neuronal activity to behavioral outcomes .

74 As noted there are still no treatments for the consequences of TBI. Endocannabinoids are
75 lipid mediators that exert a fine tuning of synaptic homeostasis¹⁹⁻²² and exhibit anti-
76 inflammatory properties^{23,24}. A critical feature of this neuromodulatory system is an on-
77 demand synthesis and release²⁵ (*i.e.* as a function of cellular activity). As endocannabinoids
78 are also tightly regulated by their degradation, pharmacological inhibition of endocannabinoid
79 degradative enzymes has been proposed as a potential therapeutic approach for the
80 treatment of TBIs^{10-12,26,27}. Nonetheless, therapeutic preclinical studies mainly during the
81 early phase of primary injury (*i.e.* minutes after injury), relied on the anti-inflammatory
82 properties of endocannabinoids. In clinical practice, patients are rarely seen in that time-
83 window, especially considering concussions/mTBIs, when patients seek care only after the

84 development of post-concussive symptoms. This left unanswered the critical question of
85 whether treatment is still possible in the later chronic phases of injury.

86 Here we show in a pediatric mouse model that a single concussion triggers long lasting
87 consequences to sensory integration in somatosensory cortex and alters associated
88 behaviors. This is due to a higher level of neuronal activity in GABAergic neurons of the
89 somatosensory cortex that blunts behaviorally-induced sensory integration. We also provide
90 evidence that pharmacological intervention is still possible when symptoms are already set in
91 the time and that the endocannabinoid system could represent an innovative approach for
92 treatment of long-term post-concussive symptoms.

93 Results.

94 **Consequences of an early life concussion on somatosensory cortex activity, plasticity** 95 **and related behaviors.**

96 Long-term consequences of an early in life brain alteration on neuronal activity were
97 assessed using the Closed-Head Injury with Long-term Disorders (CHILD) model²⁸ that
98 exhibits behavioral and morphological alterations up to 12 months^{18,29}. Mice received a
99 single mild impact at P17 in the CHILD group (CHILD group, n=4) while sham mice
100 underwent the same procedure without impact (n=5, Fig.1). We next induced a month later
101 the expression of the calcium indicator GCaMP6f in GABAergic neurons from layers 2/3 and
102 4 of the somatosensory cortex (SSC, see methods, Fig. 1, Fig 2d) and implanted through a
103 gradient refractive index (GRIN) prism (Fig.1). The correct location in the SSC of the implants
104 was later confirmed from post-mortem in MRI scans (Extended data Fig. 1).

105 With this model we first investigated the consequences of a single concussion on neuronal
106 activity in an empty housing-type cage, in absence of significant sensory stimulation (Fig.
107 2a). Two months post injury (MPI), CHILD mice exhibited a significant $88 \pm 20\%$ increase in
108 calcium-related events frequency (unpaired t-test, $p < 0.05$) when compared to their sham
109 controls (Fig. 2b, c). Strikingly, this increased activity in the somatosensory cortical neurons
110 persisted up to a year post injury (2-way RM ANOVA, $F_{(1,28)} = 8,064$, $p < 0.05$). Post-mortem
111 immunohistochemistry analysis revealed that 99% and 94% of the neurons expressing
112 GCaMP6f in sham and CHILD mice respectively, colocalized with GAD67 immunolabelling
113 (Fig. 2e), suggesting that the vast majority of transfected neurons were GABAergic. The
114 cortico-thalamo-cortical network plays a critical role in the flow of information between the
115 thalamus and sensory areas of the cortex³⁰. Thalamocortical projections undergo structural
116 reorganization without laminar-specific targeting following TBI in more mature or severe
117 preclinical models³¹⁻³³. Tractography analysis was therefore performed from *ex vivo* diffusion-
118 MRI for each group at 12 months after concussion. Overall, and in accordance with previous
119 reports from TBI models³¹, thalamocortical projections tended to be less dense (-17%) and
120 more widespread within the SSC after a single concussion (sham span of 21 ± 1 mm, CHILD
121 span of 24 ± 1 mm, n=3 per group, unpaired t-test, $p = 0.098$, Extended data table 1). In
122 addition, analysis found that thalamocortical fibers were predominantly oriented with an angle
123 with the pial surface of the SSC ($65 \pm 6^\circ$, n=3), this was shallower in CHILD brains ($54 \pm 3^\circ$,
124 n=3, Fig. 2f). These altered cortical projections have been previously linked to hyperactivity
125 of the thalamo-cortical networks³¹, suggesting a potential mechanism.

126 Mice were then challenged in the elevated plus maze at 3 months after injury (Fig. 3a). While
127 sham mice spent more time in closed arms (163 ± 27 seconds) rather than open ones ($78 \pm$
128 20 seconds, paired t-test, $p = 0.031$). After a single concussion, mice spent an equal amount
129 of time in both types of arms (118 ± 17 seconds in closed arms and 114 ± 17 seconds in
130 open arms, paired t-test, $p = 0.995$, Fig. 3b). While a differential preference for the type of
131 arms in the elevated plus maze is usually interpreted as a change in the anxiety state of the
132 animal, a lack of discrimination could as well represent the hallmark of altered sensory
133 integration after an early in life concussion. When focusing on the z-score of calcium-related
134 fluorescence of individual cells, the entry into the open arms in sham mice was associated
135 with increased cell fluorescence across the entire SSC depth (Fig. 3c). Accordingly, overall
136 SSC neuronal activity exhibited a transient and significant increase in the frequency of
137 calcium-related events at the time of the entrance of the sham animal in open arms (Fig. 3d).
138 This transient rise in SSC activity appeared to be important for the detection of the change in
139 environment, as its amplitude was negatively correlated to the number of entries in the open
140 arms made by the animals (linear regression by Pearson's correlation, $p < 0.05$, Fig. 3e, see
141 also Fig 4i and Extended data Fig 3c). In sharp contrast, we found no change of fluorescence

142 (Fig. 3c) or cortical neuronal activity (Fig. 3d) in mice from the CHILD group, suggesting the
143 absence of sensory integration upon entrance into open arms. This lack of cortical plasticity
144 induced by the change in environment in CHILD animals could therefore account for the
145 higher of number of entries in those arms compared to the sham group. Altogether our
146 results indicate that a single early in life concussion triggers a long term (*i.e.* at least up to a
147 year post-injury) cortical hyperactivity (Fig. 2c) and altered behaviorally-induced cortical
148 plasticity (Fig. 3f, 2-way RM ANOVA, sham vs CHILD regardless of the time point, $F_{(1,23)}$
149 =21.309, $p=0.004$). Those alterations in the SSC are also directly associated to a change in
150 the behavior of the animals.

151 **Endocannabinoid-mediated mitigation of the long-term effects of an early concussion.**

152 Such an increase of the neuronal activity of the somatosensory cortex after an early
153 concussion is predicted to prevent further increases in the activity, consequently blunting
154 sensory integration at the time of sensory stimulation. To test this hypothesis, we next
155 investigated the possibility of reducing the spontaneous neuronal activity to rescue
156 behaviorally-induced plasticity. The endocannabinoid system is a major neuromodulatory
157 system with anti-inflammatory properties and neuroprotective effects both *in vitro* and *in vivo*
158 ^{34,35} and is widely described in the somatosensory cortex^{36–39}. Furthermore,
159 endocannabinoids are released on-demand in an activity-dependent fashion²⁵ and can set
160 the level of activity of neuronal networks²¹. From these unique properties we predicted that
161 increasing endocannabinoid levels would reduce neuronal activity in the most active
162 networks (*i.e.* observed in the CHILD group), while inducing marginal effects on less active
163 neuronal networks (*i.e.* in the sham group). Therefore, we injected CHILD and sham mice at
164 12 months post-injury with JZL¹⁸⁴ (18 mg/kg, IP), a specific monoacylglycerol lipase blocker
165 that inhibits 2-AG degradation for several hours *in vivo*⁴⁰ and therefore increases
166 endocannabinoid availability (Fig. 4a).

167 Thirty minutes after JZL¹⁸⁴ injection, the calcium-related neuronal activity of the
168 somatosensory cortex remained unchanged in the home cage in sham animals (Tukey
169 *posthoc* test, $p>0.05$, Fig. 4b, c and Extended data Fig. 4a). In contrast, when injected with
170 JZL¹⁸⁴, CHILD animals exhibited a decreased calcium-related neuronal activity in the SSC in
171 absence of significant sensory stimulation (Tukey *posthoc*, $p<0.05$), that matched the level of
172 activity of sham animals (tukey *posthoc*, $p>0.05$, Fig. 4b, c and Extended data Fig. 4a).
173 Hence, in absence of substantial sensory stimulation, JZL¹⁸⁴ reduced the calcium-related
174 neuronal activity of the somatosensory cortex of CHILD animals but not shams (2-way RM
175 ANOVA, $p<0.05$, Fig. 4c).

176 We next tested the consequences of calcium-related neuronal activity normalization in
177 CHILD mice on elevated plus maze-induced neuronal plasticity. We found that in presence of
178 JZL¹⁸⁴ calcium-related neuronal responses induced by the entry into open arms was rescued
179 in CHILD mice (Fig. 4d and 4f). This was also associated with no difference between groups
180 in the number of entries into the open arms (sham+JZL vs CHILD+JZL, unpaired t-test,
181 $p>0.05$, Fig. 4e). JZL benefit was both specific and reversible as vehicle injection a week
182 later failed to reproduce JZL effects in the test (Fig.4g). We also found that neuronal
183 responses observed across all sessions in the somatosensory cortex was highly predictive of
184 the behavioral outcomes (*i.e.* the number of entries in the open arms) in the elevated plus
185 maze (Fig. 4h and 4i). Using a classification algorithm to segregate sham from CHILD
186 animals, based on basal network activity (in the home cage), amplitude of the neuronal
187 network's response to the entry of the open arms of the elevated plus maze and the number
188 of entries of the animals in the open arms as modalities obtained at 6 and 9 MPI, we were
189 able to correctly classify all the animals during the vehicle injection experiment at 12 MPI
190 (loss of 0.1019 and accuracy of 1). Remarkably, when tested on the JZL injection dataset,

191 the algorithm misclassified all CHILD animals as sham animals (loss of 6.0792 and accuracy
192 of 0.5), further supporting the rescue of the phenotype by the JZL injection. These results
193 strongly support that CHILD effects on neuronal activity, plasticity and associated behaviors
194 that can be reversibly dampened a year after injury with the pharmacological intervention of
195 the specific endocannabinoid degradation inhibitor JZL¹⁸⁴.

196 **Behaviorally-induced potentiation of neuronal activity alteration is a hallmark of early** 197 **in life concussion.**

198 We also investigated whether other behaviors associated with cortical somatosensory
199 integration are impacted 6 months after early in life concussion. In the novel object
200 recognition task, exposure to the novel object was shown to induce an increase in the activity
201 of the somatosensory cortex, specifically in layers 2/3⁴¹. In order to determine whether an
202 early in life traumatic experience would blunt other forms of neuronal potentiation, we tested
203 the ability of mice to exhibit novel object-induced neuronal potentiation. For this purpose,
204 mice were first habituated to the empty open field for 5 minutes and then to 2 identical
205 objects for 5 minutes the following 3 days. On the test day, one of the familiar objects was
206 substituted for a new one. Under these conditions, sham mice exhibited an increased interest
207 for the novel object as expressed by an increased preference index (tukey *posthoc*, $p < 0.05$,
208 Fig. 5b). As previously described, neuronal activity in the most superficial layers of the SSC
209 (layers 2/3, Fig. 5a) was specifically increased (top plots of Fig. 5c). In contrast, mice that
210 suffered early in life concussion did not exhibit any particular interest for the novel object
211 (tukey *posthoc*, $p > 0.05$, Fig. 5b), which was highly different from the sham population (2-way
212 RM ANOVA, $p < 0.05$, Fig. 5b). This absence of interest for the novel object was also
213 associated with an absence of specific neuronal response of the SSC induced by the switch
214 in objects (bottom plots of Fig. 5c).

215 We next evaluated the consequences of an early in life injury on sensory motor integration in
216 the beam walk task. Overall, sham and CHILD mice performed equally in terms of time to
217 cross 30 cm beams (Extended data Fig. 4c), regardless of the diameter of the beam (2-way
218 RM ANOVA, $p > 0.05$, Extended data Fig. 4c), suggesting the absence of major locomotor
219 dysfunctions. However, CHILD mice exhibited an increased number of slips (errors) from of
220 the right hind paws compared to the shams (unpaired t-test, $p < 0.05$, Fig. 5d). Remarkably, in
221 sham mice right hind-paw errors were associated with an increase in calcium-related
222 neuronal activity (Fig. 5e and 5f) signifying somatosensory integration. After early in life
223 concussion, mice hind-paw errors did not correlate to a change in calcium-related neuronal
224 activity (Fig. 5e and 5f), suggesting a deficit in sensory processing in the SSC after CHILD
225 (2-way RM ANOVA, $p < 0.05$, Fig. 5f). Mice were also tested on the rotarod paradigm to
226 further assess sensory motor integration. Sham mice performed better than CHILD mice,
227 reaching a higher speed on the rotarod before falling (unpaired t-test, $p < 0.05$, Fig. 5g).
228 Gradual increase of rotarod speed correlated to increased calcium-related activity in neurons
229 of the SSC in sham group (calcium events frequency at 4RPM vs calcium events frequency
230 at max speed in sham mice, paired t-test, $p < 0.05$, Fig. 5h). In contrast, the calcium-related
231 activity of the neurons in the SSC did not change with increased rotarod speed in the CHILD
232 group (calcium events frequency at 4RPM vs calcium events frequency at max speed in
233 CHILD mice, paired t-test, $p > 0.05$, Fig. 5h and Extended data Fig. 5). This further
234 strengthens the hypothesis that mice with early in life concussion were unable to increase
235 neuronal activity in the SSC for proper sensory motor integration (see also Extended data
236 Fig. 5). We also show that regardless of the experimental group the neuronal activity in the
237 SSC at the minimal speed (4 RPM) was highly predictive of the performance of the mice on
238 the rotarod (Pearson's correlation, $p < 0.05$, Fig. 5i).

239 Our results clearly demonstrate that sensory integration in SSC, and associated behaviors,
240 are dampened after early in life brain concussion when sensory integration is associated to
241 an increase in activity in this cortex.

242 **Specificity of the alteration of plasticity induced by an early life traumatic brain injury.**

243 We next investigated whether a CHILD is also associated with alterations of forms of short-
244 term depression of neuronal activity. We found that sham mice positioned on a slightly
245 heated plate (from 20 to 26°C) for 30 s exhibited a significant overall decrease in calcium-
246 related neuronal activity in the SSC ($-73 \pm 2\%$ from control activity at 20°C, $p < 0.001$, Fig. 6).
247 Under identical experimental paradigm, CHILD mice presented a similar (2-way RM ANOVA,
248 $p > 0.05$,) decrease in calcium-related neuronal activity ($-67 \pm 2\%$ from control activity at 20°C;
249 $p < 0.05$, Fig. 6), suggesting that depression of neuronal activity to thermal stimuli remains
250 unaltered after early in life concussion.

251 Discussion.

252 It is well established that traumatic brain injuries are associated with long term alterations in
253 a broad range of physiological functions, even for mild severity, including sensory alterations,
254 contributing to worsening of the patient's quality of life. To date, the neuronal mechanisms
255 triggered by such events are poorly understood, especially regarding the long-term
256 consequences for which no existing treatment exists for these patients. While children
257 represent the most susceptible population to suffer TBIs, specific research on long-term
258 consequences of those events on the brain that is in development is scarce^{42,43}. In our
259 CHILD model, we previously showed long-term behavioral dysfunctions were associated with
260 neuronal loss at 12 months in the hippocampus¹⁸. However, the neuronal activity has never
261 been assessed over time following the injury in the same individuals. Our novel and timely
262 findings demonstrate for the first time that: **(1)** early in life concussion durably disturbs basal
263 neuronal activity in the SSC at the site of impact, even without overt loss of neurons, **(2)**
264 SSC-neuronal hyperactivity is associated with altered sensory-dependent potentiation of the
265 activity of this network and its related behaviors, **(3)** these alterations are specific to
266 potentiation of neuronal activity since sensory-dependent depression of the activity remains
267 possible, and finally that **(4)** reducing SSC neuronal-activity *via* the potentiation of the
268 endocannabinoid signaling rescues both neuronal plasticity in the SSC and the correlated
269 behaviors. Broadly, we show that the rescue of alterations induced by a concussion during
270 early stages of brain development could be reached a year after injury, which represents a
271 dramatically expanded therapeutic window that is much more amenable for clinical
272 intervention than within minutes after injury, as previously suggested^{10-12,44}. Our study also
273 further extends the interest of the endocannabinoid system as a potent and future
274 therapeutic target in the treatment of traumatic brain injuries^{10-12,27,34,44-48} and possibly other
275 brain injuries such as stroke⁴⁹, or neurodegenerative diseases^{27,50}.

276 A crucial feature of traumatic brain injuries is that anyone in its lifetime can suffer one. While
277 severe injuries typically lead to heavy behavioral consequences to the patient, the vast
278 majority of TBI are considered mild. Most mTBI patients do not enter typical hospital
279 emergency rooms and if so are typically quickly discharged with no clinical following.
280 Epidemiologic studies indicate that about 20% of adults suffering mTBIs will eventually
281 develop symptoms lasting 3 months or more^{2,3}. When considering the precocity of injury, the
282 incidence of adverse outcomes increases. First, children aged 0 to 4 years old represent one
283 of the two most at-risk age-class⁵¹. Second, it is estimated that when suffering a mTBI,
284 children more susceptible than adults to developing long lasting consequences^{4,5,52,53}.
285 Previous reports have shown in juvenile animal models of severe TBIs, an increased
286 neuronal activity in the ipsilateral somatosensory cortex¹⁶ and hippocampus¹⁷ during the sub-
287 acute phase of the injury (*i.e.*, up to a month post injury). Our work demonstrates for the first
288 time that a single, mild, early in life event triggers long-lasting (*i.e.* at least 12 months post-
289 injury) perturbations of brain network activity and related behaviors. Our results strengthen
290 previous observations in mild juvenile brain injury, showing changes in electro-
291 encephalographic activity within gamma frequency at 1 month post-concussion⁵⁴ and
292 memory dysfunction related with a loss of neurons in the hippocampus at 12 months¹⁸. We
293 also previously observed remote alterations, outside of the central nervous system with long-
294 term cardiac dysfunction²⁹. These studies strongly argue for the need for a deeper and more
295 sustained follow-up of younger patients over the long-term. In clinics, traumatic brain injuries
296 during adulthood have been associated to an increased incidence of neurodegenerative
297 disorders including chronic traumatic encephalopathies, Alzheimer's and Parkinson's
298 diseases⁵⁵. In Parkinson's preclinical models, an increased neuronal activity in the amygdala
299 or substantia nigra have been associated with an increased vulnerability to develop disease-
300 related symptoms^{56,57}. Further studies are therefore required to investigate whether the early

301 concussion -induced hyperactivity we report here in the somatosensory cortex could
302 potentially contribute to progression of neurodegenerative disorders. This also raise the
303 importance of long-term studies in regard of early traumatic brain injuries to understand the
304 multiplicity of mechanisms at play when long-term symptoms develop in order to develop *ad*
305 *hoc* and targeted therapeutic strategies.

306 We found that neuronal plasticity of SSC neurons was specifically blunted when it requires
307 increasing neuronal activity. Our findings rely on neuronal plasticity of the SSC induced while
308 the animal is behaving in a paradigm that we designed to exhibit a strong sensory
309 component. Taken individually, and without the parallel use of *in vivo* calcium imaging, these
310 tests could lead to different interpretations, but taken together rather indicate altered sensory
311 processing. For instance, we found that mice that entered the open arms of elevated plus
312 maze presented a significant transient increase in neuronal activity in the somatosensory
313 cortex. The amplitude of this form of plasticity was directly inversely correlated to the number
314 of entries in the open arms (Fig. 3e and Fig. 4i). To our knowledge, this is the first report of
315 this behaviorally-induced form of short-term potentiation of neuronal activity. Dogmatically, a
316 change in the number of entries in the open arms in the elevated plus maze is interpreted as
317 a change in the anxiety level of the animal. We propose that after early in life traumatic brain
318 injury the mice in our experimental conditions were not less anxious, but rather were not able
319 to properly integrate a change in environment (i.e. transitioning from closed to open arm),
320 thereby blunting the anxiogenic properties of the edge. Further work is required to determine
321 whether this form of plasticity is related to sensory integration induced by motion and
322 whisking of the animal⁵⁸.

323 The specific neuronal responses of layers 2/3 but not layer 4 of the S1 somatosensory cortex
324 induced by the novel object has been described previously⁴¹. We found that after an early in
325 life concussion mice failed to show an increased interest for the novel object and the
326 neuronal plasticity induced by its presence was blunted. Traditional interpretation of these
327 results would suggest an alteration of recognition memory. In the context of our behavioral
328 approach, we rather interpret these results as the consequence of a loss of sensory
329 integration facilitating object recognition.

330 The SSC has been implicated through sensory integration in the early stages of motor skill
331 acquisition in humans⁵⁹⁻⁶¹. We found that while sham mice were crossing beams in the
332 eponym task, errors in the right hindpaw positioning were associated with transient neuronal
333 responses in the SSC, suggesting specific neuronal error-related sensory integration. In
334 CHILD mice no response was observed while the errors occurred, suggesting an absence of
335 error-related sensory integration and that could impede motor skill acquisition in the task,
336 therefore leading to the increased number of errors made. We also found that neuronal
337 activity in the somatosensory cortex increased in correlation with the speed of the rotarod in
338 the first trial of the test. Interestingly we found that under that experimental condition the level
339 of activity at the beginning of the test (i.e. 4 RPM) was predictive of the performance of the
340 mice to stay on the rotarod when speed was increasing. Our novel observations suggest that
341 this neuronal network is able to perform sensory integration in order to adapt locomotion to
342 the rod-speed until reaching a saturated level of activity, at which point the motor command
343 becomes inadequate, leading to the fall of the animal. This would explain the early fall of
344 mice after early in life concussion that present with an already high basal level of neuronal
345 activity. Interestingly, once learned the performance in the task appeared to become
346 independent of somatosensory cortex activity as the correlation was lost on the next test 3
347 months later (data not shown). As a consequence, sham and CHILD performed equally on
348 this subsequent test. This would argue that during the acquisition phase of the task,
349 performance requires correct sensory integration in the somatosensory cortex, which once

350 learned, the generation of the most appropriate walking behavior relies on other brain
351 structures likely not affected in our model. This interpretation adds to the view that
352 movement-related somatosensory feedback encoded in S1 is important for correct paw
353 positioning and ultimately performance⁶².

354 Thermal integration on the somatosensory cortex had been previously described^{63–65}. The
355 most recent of these studies aimed at deciphering the cellular encoding of focal thermal
356 information, *i.e.* within seconds following the exposure. Our experimental set up did not allow
357 for such time and space resolution. Rather we analyzed neuronal activity over the 30
358 seconds of exposure to increased temperature of the heating pad and unmasked a
359 depression of the activity of the somatosensory cortex. Such a depression of neuronal
360 activity had been described in rats, with local heat to the scrotal skin⁶⁵. Therefore, the
361 depression of the activity of neurons in the somatosensory cortex we describe here could be
362 attributed to a rebound inhibition following the thermal change or to the overall thermal
363 encoding of all the skin patches exposed on the heating pad (skin patches of the fore and
364 hindpaws, belly, and/or scrotum). In that experimental context, both sham and CHILD mice
365 exhibited similar responses. This would argue for the hypothesis that only sensory integration
366 requiring an increased neuronal activity is altered by an early in life concussion.

367 Highlighting the need for interpretation of behavioral paradigms in their context rather than
368 according to dogmatic interpretations, we found previously unappreciated alterations of
369 neuronal plasticity in the SSC after early in life concussion, and this lasted up to a year after
370 the concussion. These alterations were specific to increases in neuronal activity as exposure
371 to an increase in 6°C induced a reduction in SSC calcium-related neuronal activity that was
372 similar in both groups. Our hypothesis is that the increased activity either acts as neuronal
373 noise that prevents proper sensory integration (*i.e.* change in inputs) or saturates cellular
374 firing, making impossible further increase in activity with a ceiling effect (*i.e.* change in
375 cellular properties). Our pharmacological manipulation of the endocannabinoid system
376 supports the later hypothesis. Endocannabinoids are critically involved in both synaptic
377 transmission regulation^{19,20} and cell excitability (notably regulating GIRK channels and Ih
378 currents^{66–69}). While both actions would explain the reduction in basal activity following
379 endocannabinoid degradation inhibition, a reduction in synaptic inputs induced by an
380 endocannabinoid tone increase in those conditions could not explain neuronal potentiation
381 rescue, unless through a dis-inhibition mechanism.

382 Our study also addresses the fundamental question of whether the long-term changes
383 induced by early in life event can be reversed by an intervention that is amenable within a
384 clinical setting. While blocking endocannabinoid degradation within minutes of injury had
385 been proposed as a treatment in more mature preclinical models, relying on the anti-
386 inflammatory properties of endocannabinoids to prevent the development of the primary
387 injury^{10–12,44}, we tested such treatment at time from injury when post-concussive symptoms
388 have already developed (*i.e.* a year after concussion). We found that modulating this system
389 according to that protocol could successfully rescue basal neuronal activity and neuronal
390 plasticity in the somatosensory cortex and the associated behaviors. While definitively
391 showing that this rescue was due to the pharmacological agent, the fact that when tested a
392 week later with a vehicle injection, animals exhibited again the post-concussive deficits
393 brings up a limitation of that approach with the question of the treatment efficacy duration.
394 Further work is therefore critical to identify an optimal drug exposure (dose, frequency) that
395 would infer durably a reversal of these post-concussive symptoms. In addition, the
396 endocannabinoid release is tightly linked to neuronal activity^{20,70}. Targeting their degradation
397 presents an advantage to firstly regulate the most active neuronal networks, minimally

398 disturbing those with low to normal levels of activity. As a consequence, this strategy is
399 expected to minimize off-target effects.

400

401 Sensory integration is a major component of brain processing to allow adaptation to the
402 environment and to ensure survival. One common thought is that events early during brain
403 development have a minimal impact on brain function because of the relatively high plasticity
404 capacity of the immature brain. Clinical studies reveal that pediatric traumatic brain injuries
405 can lead to long-term post-concussive symptoms^{4,5}, a persistent increase in basal brain
406 activity associated to blunted plasticity is a previously unappreciated mechanism for the
407 development of long-term alterations of behaviors post-injury (*i.e.* symptoms). Targeting
408 basal neuronal activity could provide an innovative therapeutic strategy to prevent the
409 development of post-concussive symptoms following an early in life concussion. Future work
410 should evaluate the relevance of the blockade of the activity-dependent modulation of
411 endocannabinoid degradation.

412 **Acknowledgements.**

413 This research project was funded by Eranet Neuron MISST and Neuvasc (JB), Agence
414 Nationale de la recherche (JB), Nanospace (JB) and NIH, Grant No. (1R01NS119605-01 AO
415 and JB). We thank Richard Rouland and Jonathan Zapata for experimental advice and
416 helpful discussions.

417

418 **Author contribution.**

419 JB designed the experiments, interpreted the results and proofed the manuscript. LH
420 performed CHILD and all MRI scans. MM performed immunohistochemistry. BPN analyzed
421 MRI scans and tractography. AO designed the experiments, interpreted the results and
422 proofed the manuscript. C.J.D. designed and performed the experiments, the analysis and
423 interpretation of the data and wrote the manuscript.

424

425 **Author information.**

426 Reprints and permissions information is available at www.nature.com/reprints. The authors
427 declare no competing financial interests. Correspondence and requests for materials should
428 be addressed to CJD (christophe.dubois@u-bordeaux.fr).

429 Figure legends.

430

431 **Figure 1. Experimental protocol.**

432 Seventeen days after birth, mice from the CHILD group received a single mild traumatic brain
433 injury, while animals from the sham group followed the same procedure at the exception of
434 the impact. A month later, injections of a virus allowing the expression of GCamp6F under
435 the CamK2a promoter were performed in the somatosensory cortex of all mice and the GRIN
436 lens were implanted at the same location. Every 3 months following TBI, neuronal
437 somatosensory cortex activity of all animals was evaluated without significant sensory
438 stimulation (in a typical home-cage) or while on an elevated plus maze. At the 6-month post-
439 injury time point, animals were also probed with the novel object recognition task, beam walk
440 task, rotarod and hot plate test. All these tests were designed to focus on sensory
441 integration. One year after concussion, the effects on endocannabinoid degradation inhibition
442 were pharmacologically tested in a home-cage and elevated plus maze. *Ex vivo* MRI and
443 immunohistochemistry experiments were then performed.

444 **Figure 2. Consequences of an early life concussion on somatosensory cortex activity 445 and imaging.**

446 **a.** While in a typical home-cage, calcium imaging in the somatosensory cortex was
447 performed *in vivo* in unanesthetized mice. **b.** Representative $\Delta F/F$ calcium recordings from
448 sham and CHILD mice. **c.** Twelve-month time course of calcium events frequency in
449 somatosensory cortical neurons (Hz) in sham (n=5) and CHILD mice (n=4). CHILD mice
450 exhibited a significant increase in activity in those neurons regardless of the time point (2-
451 way RM ANOVA, $F_{(1,28)}=8.064$, $p=0.025$). **d.** Typical Gcamp6f fluorescence at low (left) and
452 high (right) magnifications. The white notch represents the GRIN lens location. **e.**
453 representative fluorescence images of Gcamp6f and GAD₆₇-immunofluorescence in sham
454 (top) and CHILD (bottom) animals. GAD₆₇-immunofluorescence was found in 99% of the
455 sham neurons evaluated (158/159, in 3 animals) and in 94% of the CHILD neurons (147/156,
456 in 3 animals). **f.** DTI tractography mapped from the left medial ventral posterior lateral
457 nucleus (VPLM) of the thalamus and terminating in the somatosensory cortex (SSC). As can
458 be visualized, CHILD mice tended to exhibit lower density fiber (n=3 for both groups, $p>0.05$,
459 see extended data table 1), an increased tract dispersion between the VPLM and the SSC
460 (n=3 for both groups, $p>0.05$, see extended data table 1) and a shallower entry angle in the
461 SSC (n=3 for both groups, $p>0.05$, see extended data table 1). Average values are shown as
462 solid lines, SEM is represented as the shaded area. *, $p<0.05$.

463 **Figure 3. Consequences of an early life concussion on somatosensory cortex 464 plasticity induced by sensory integration in the elevated plus maze.**

465 **a.** While on an elevated plus maze, calcium imaging in the somatosensory cortex was
466 performed *in vivo* in unanesthetized mice. **b.** Group data showing the time spent in open and
467 closed arms of the elevated plus maze for sham (n=5) et CHILD (n=4) mice. While sham
468 mice spent more time in the closed arms (163 ± 27 s vs 78 ± 20 s in open arms, paired t-test,
469 $p=0.031$), CHILD spent indistinctly the same amount of time in each type of arm (open arms
470 114 ± 17 s, closed arms 118 ± 17 s, paired t-test, $p=0.995$). **c.** z-score plots of representative
471 sham and CHILD animals with cells ordered in function of their depth in the somatosensory
472 cortex (with the deepest cells at the bottom). Plots are averages of 3 to 5 events and
473 centered to the entrance of the animals into the open arms of the maze (dashed lines).
474 Increased neuronal activation at the entrance is seen in sham animals (in red, after the dash
475 line) but not in CHILD mice. **d.** Average plots of the averaged normalized calcium-transients
476 frequency of sham (grey, n=5) and CHILD (purple, n=4) groups. A significant increase in
477 neuronal calcium activity occurred at the entrance in the open arms (red dash line) in sham

478 mice ($+136 \pm 23\%$, paired t-test, $p=0.039$) but was blunted in CHILD mice ($+37 \pm 28\%$,
479 paired t-test, $p=0.747$). **e.** Scatter plot of the number entries in the open arms plotted vs the
480 amplitude of the increase in calcium-transients frequency in sham (grey, $n=5$) and CHILD
481 (purple, $n=4$) mice. Overall an inverse relationship was found between these 2 parameters
482 (Pearson's correlation, $p=0.049$, see also panel i in figure 4). **f.** Twelve-month time course of
483 calcium events frequency increase at the entrance in the open arms in somatosensory
484 cortical neurons in sham ($n=5$) and CHILD mice ($n=4$). CHILD mice exhibited a blunting of
485 this form of neuronal sensory integration in those neurons regardless of the time point (2-way
486 RM ANOVA, $F_{(1,23)}=21.309$, $p=0.004$). Average values are shown as solid lines, SEM is
487 represented as the shaded area (error bars in b.). NS, $p>0.05$, *, $p<0.05$, ** $p<0.01$.

488 **Figure 4. Endocannabinoid-mediated mitigation of the long-term effects of an early life**
489 **concussion.**

490 **a.** Experimental procedure for the pharmacological intervention 12 months after the TBI
491 using a specific inhibitor of endocannabinoid degradation induced by the monoacylglycerol
492 lipase (JZL¹⁸⁴, 18 mg/kg). **b.** and **c.**, calcium-related neuronal activity in the somatosensory
493 cortex recorded in a typical home-cage, 30 minutes after an IP injection of JZL¹⁸⁴. **b.**
494 Representative $\Delta F/F$ calcium recordings from sham and CHILD mice, before (left, black and
495 purple traces, respectively) and 30 minutes following the IP injection of JZL¹⁸⁴ (right, green
496 traces). **c.** Group data showing that the potentiation of endocannabinoid signaling by JZL¹⁸⁴
497 injection specifically targeted basal calcium-related neuronal activity in CHILD mice (2-way
498 RM ANOVA, $F_{(1,15)}=10.444$, $p=0.018$, \square). JZL184 had no effect in sham mice ($n=4$, tukey
499 posthoc, $p=0.45$, NS) while it reduced calcium related neuronal activity in the somatosensory
500 cortex of CHILD mice ($n=4$, tukey posthoc, $p=0.002$, **) to sham levels ($n=4$ in both groups,
501 tukey posthoc, $p=0.364$). **d. to i.**, endocannabinoid-dependent modulation of calcium-related
502 neuronal plasticity induced by the entrance in open arms of the elevated plus maze and
503 associated behavior. **d.** z-score plots of a representative CHILD mouse 9 MPI, and 12 MPI
504 30 min after JZL184 injection and 12MPI 30 min after vehicle injection, with cells ordered in
505 function of their depth in the somatosensory cortex (with the deepest cells at the bottom).
506 Plots are averages of 3 to 5 events and centered to the entrance of the animals into the open
507 arms of the maze (dashed lines). Increased neuronal activation at the entrance is seen when
508 the animal was injected with JZL¹⁸⁴ (in red, center plot after the dash line) but not at 9MPI or
509 when injected with a vehicle solution. **e.** Group data of the number of entries in the open arm
510 by sham ($n=4$) and CHILD ($n=4$) mice 30 min after injection. Both groups exhibited the same
511 behavior (unpaired t-test, $p=0.814$). **f.** Average plots of the averaged normalized calcium-
512 transients frequency of CHILD mice at 9MPI (purple, $n=4$) and at 12 MPI 30 min following a
513 JZL184 injection (green, $n=4$). A significant increase in neuronal calcium-related activity
514 occurred in CHILD mice ($n=4$) at the entrance in the open arms (red dash line) in presence of
515 JZL¹⁸⁴ ($+99 \pm 9\%$, paired t-test, $p=0.007$, #) but not in presence of vehicle ($+13 \pm 9\%$, paired
516 t-test, $p=0.499$). **g.** Average plots of the averaged normalized calcium-transients frequency of
517 sham ($n=4$) and CHILD ($n=4$) mice at 12 MPI following a vehicle injection. Similarly to the 6
518 and 9 MPI time points without injection, a significant increase in neuronal calcium-related
519 activity was seen in sham mice ($n=4$) at the entrance in the open arms (red dash line) after
520 vehicle injection ($+106 \pm 28\%$, paired t-test, $p=0.012$, #) but not in CHILD mice ($n=4$, $+20 \pm$
521 13% , paired t-test, $p=0.194$). **h.** and **i.**, Scatter plots of the number entries in the open arms
522 plotted vs the amplitude of the increase in calcium-transients frequency at the time of entry.
523 **h.** in sham and CHILD mice 30 minutes after a vehicle injection (sham, light blue $n=4$;
524 CHILD, dark blue $n=4$), and **i.** across all the experiments performed from both groups ($n=34$).
525 Overall a significant inverse relationship was found between the amplitude of calcium-related
526 neuronal activity and the number of entries in the open arms (Pearson's correlation, $p<0.01$,

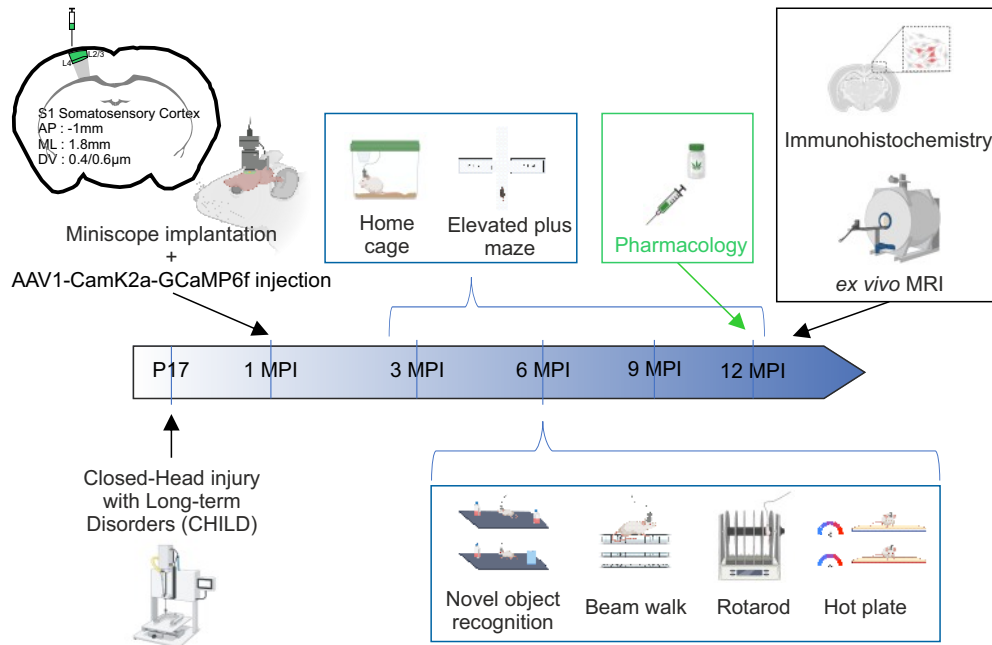
527 ***). Average values are shown as solid lines in **f.** and **g.**, SEM is represented as the shaded
528 area (error bars in **c.** and **e.**).

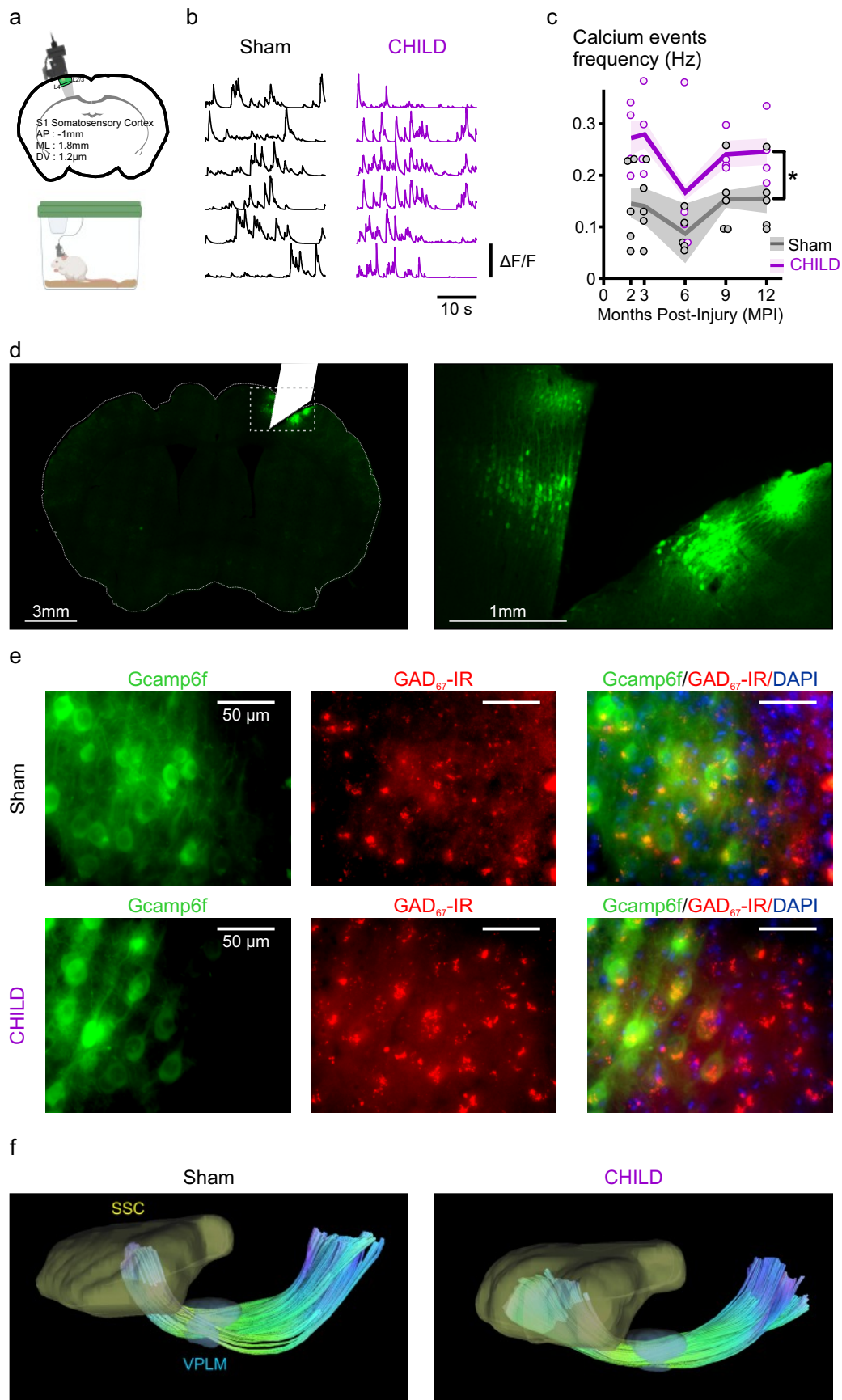
529 **Figure 5. The alteration of behaviorally-induced potentiation of neuronal activity is a**
530 **hallmark of an early life concussion.**

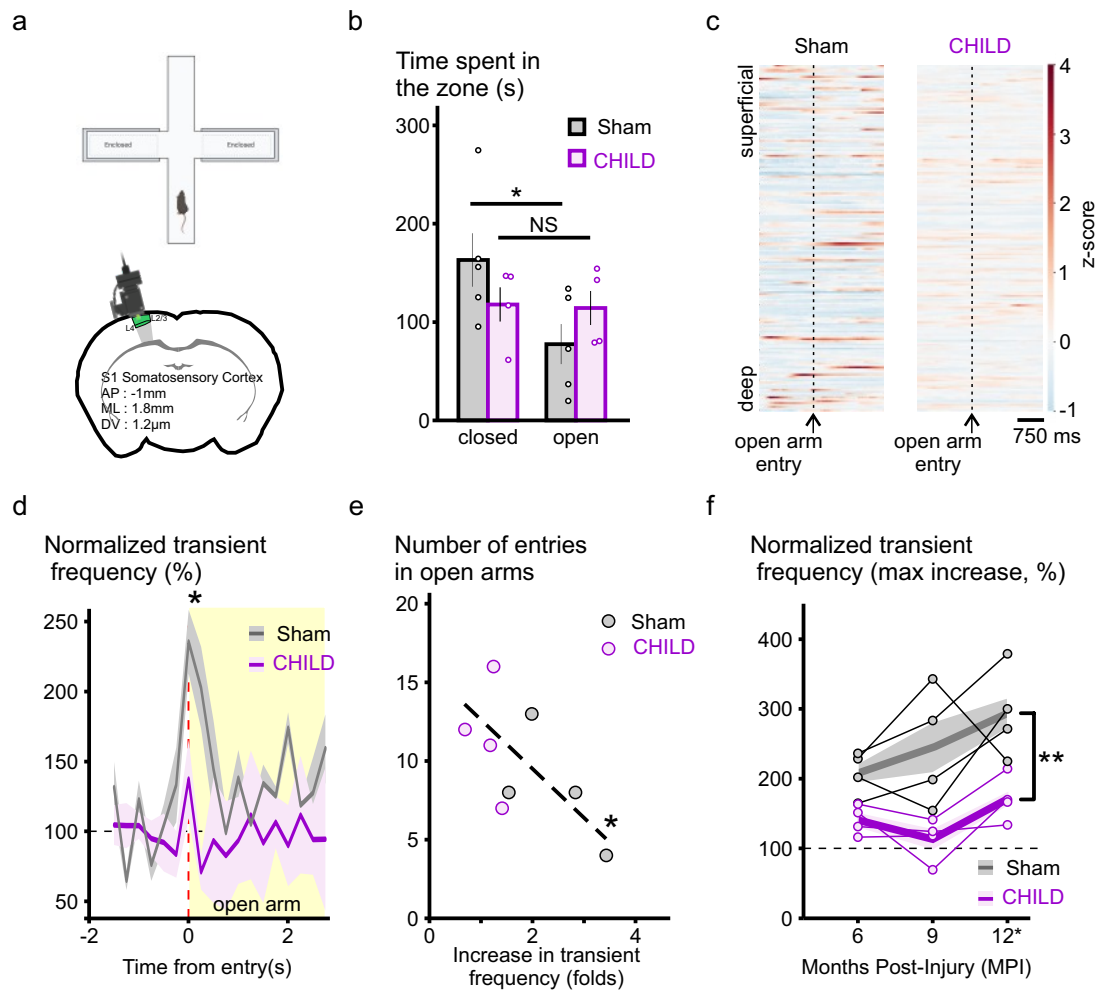
531 **a., b. and c. Novel object discrimination task.** **a.** calcium imaging was performed in the left
532 somatosensory cortex (ipsilateral to the injury when applicable). **b.** Group data of the
533 preference index for the novel object at day 5 of the protocol (see methods). Sham (n=5) and
534 CHILD (n=4) mice exhibited differences in attraction to the novel object (2-way RM ANOVA,
535 $F_{(2,23)}=1.155$, $p=0.001$, ***). Sham mice spent more time with the novel object (tukey posthoc,
536 $p<0.001$, ###) while CHILD mice did not exhibit preference (tukey posthoc, $p=0.331$, NS). **c.**
537 Whole session representative raster plots of calcium events on day 1 without object (left,
538 'openfield'), on day 4 with familiar objects (center, 'Familiar objects') and on day 5 when
539 exposed to the novel object recorded in a sham (top) and CHILD (bottom) mice. Cells are
540 organized by their depth in the cortex, with deepest cells at the bottom (orange, layer 4 of the
541 SSC) and most superficial at the top (blue, layers 2/3 of the SSC). When exposed to the
542 novel object sham mice exhibited a specific increase in calcium transients in layers 2/3 of the
543 SSC (top). In contrast CHILD mice exhibited overall higher level of calcium transient
544 frequency in all layers and did not show any change in presence of the novel object (bottom).
545 **d., e. and f. Beam walk.** **d.** Group data of the number of errors (paw slips) made by sham
546 (n=5) and CHILD (n=4) mice. CHILD mice made more paw positioning errors compared to
547 sham mice (unpaired t-test, $p=0.042$, *). **e.** z-score plots of representative sham and CHILD
548 animals with cells ordered in function of their depth in the somatosensory cortex (with the
549 deepest cells at the bottom). Plots are averages of 3 to 5 events and centered to a right
550 hindpaw slip (dashed lines). Increased neuronal activation at the error is seen in sham
551 animals (in red, after the dash line) but not in CHILD mice. **f.** Average plots of the averaged
552 normalized calcium-transients frequency of sham (grey, n=5) and CHILD (purple, n=4) mice
553 centered to the mispositioning of the right hindpaw (dashed lines). A significant increase in
554 neuronal calcium-related activity occurred in sham mice at the time of the error (paired t-test,
555 $p=0.034$, *) while this was blunted in CHILD animals (2-way RM ANOVA, $F_{(5,53)}=2.566$,
556 $p=0.044$, *). **g., h. and i. Rotarod.** **g.** Group data showing the maximum rod speed sham
557 (n=5) and CHILD (n=4) mice could handle before falling. Sham mice could handle higher
558 speeds (12.8 ± 0.3 RPM) compared to CHILD animals (9.3 ± 0.5 RPM, unpaired t-test,
559 $p=0.016$, *). **h.** Average plot of the calcium-related neuronal activity in GABAergic neurons of
560 the somatosensory cortex according to the speed of the rod. While neuronal activity
561 increased with speed in sham mice (+ 45 % from 0.12 ± 0.02 Hz to 0.18 ± 0.03 Hz at
562 maximum speed, paired t-test, $p=0.017$), it did not significantly increase in CHILD mice (+ 7
563 % from 0.27 ± 0.06 Hz to 0.28 ± 0.02 Hz at maximum speed, paired t-test, $p=0.605$). **i.** Plot
564 showing the significant inverse correlation between the calcium-related neuronal activity in
565 the SSC at 4 RPM and the maximum speed of the rod that sham (n=5) and CHILD (n=4)
566 mice could handle (Pearson's correlation, $p=0.002$, **). Average values are shown as solid
567 lines in **f.** and **h.**, SEM is represented as the shaded area (error bars in **d.** and **g.**).

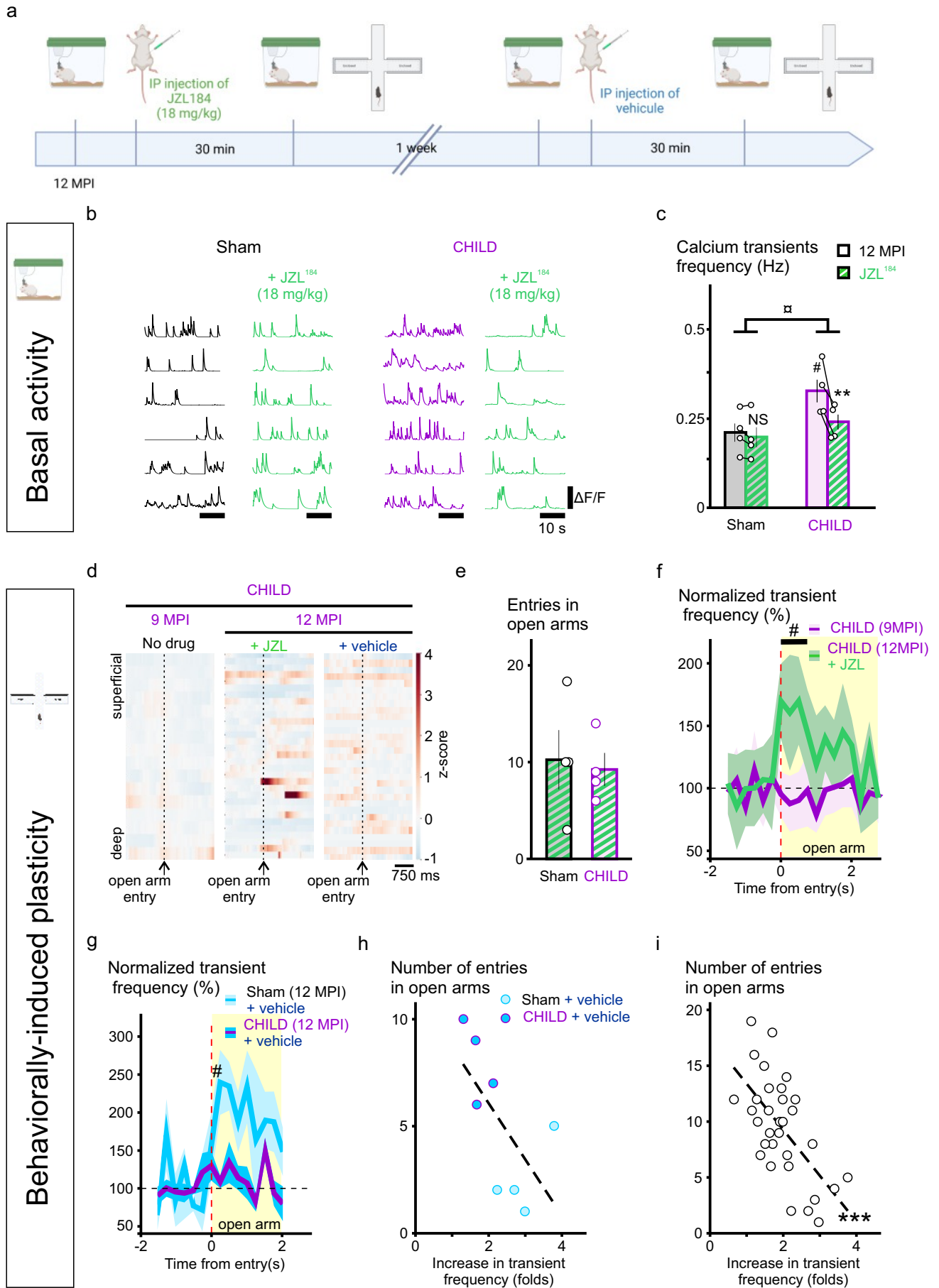
568 **Figure 6. Heat-induced decrease in calcium-related neuronal activity in the SSC**
569 **remains unaffected by an early life concussion.**

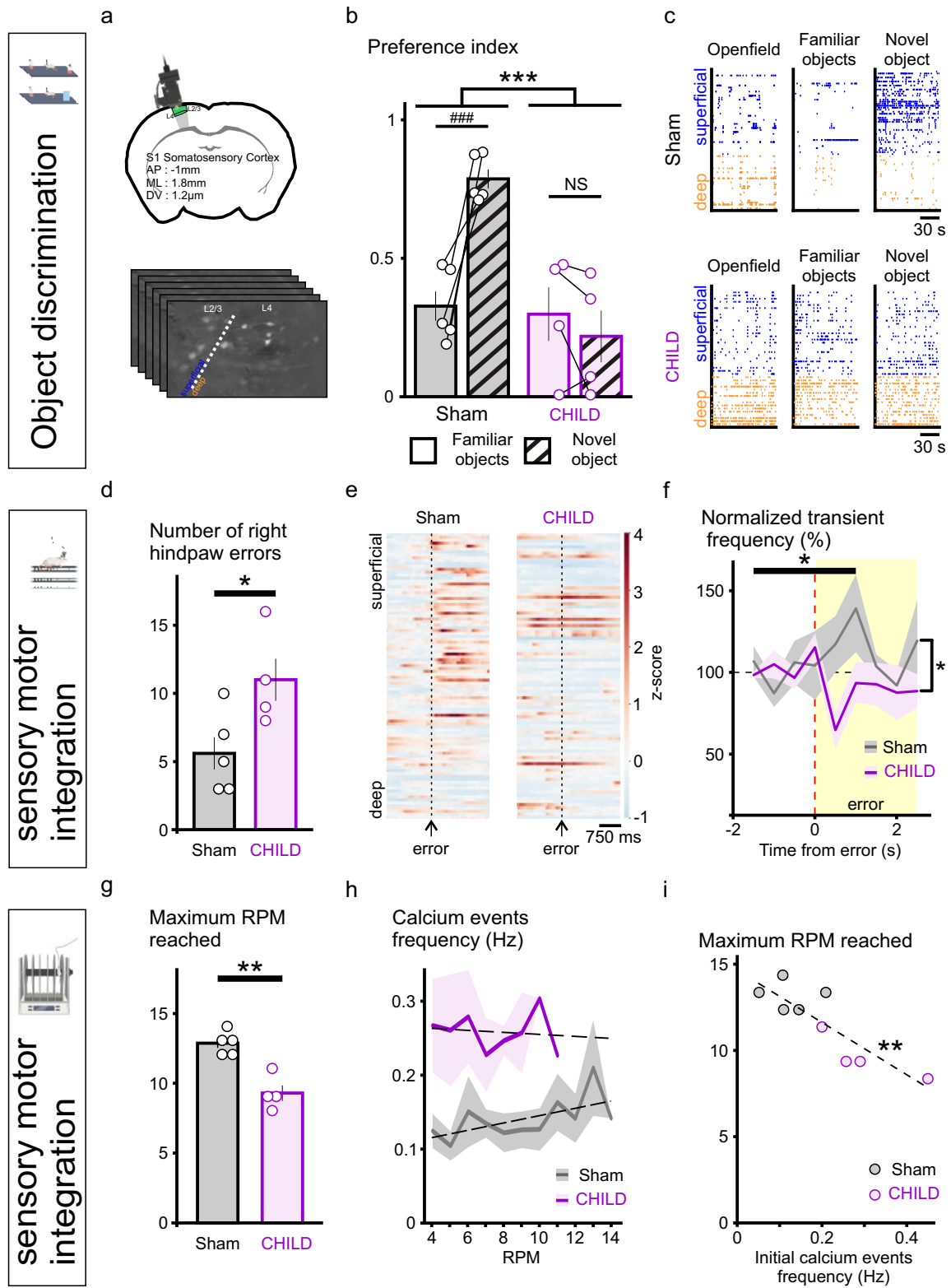
570 Group data showing that a 30 seconds exposure to a 6°C increase in floor temperature
571 induced a similar decrease in calcium related neuronal activity in the SSC in both sham (n=5)
572 and CHILD (n=4) mice (2-way RM ANOVA, $F_{(1,17)}=3.339$, $p=0.11$). sham mice exhibited a 73
573 ± 2 % decrease (from 0.14 ± 0.02 Hz to 0.04 ± 0.01 Hz, tukey posthoc, $p<0.001$, ***) while
574 CHILD mice exhibited a 67 ± 7 % decrease (from 0.26 ± 0.04 Hz to 0.09 ± 0.03 Hz, tukey
575 posthoc, $p<0.001$, ***). SEM is represented as error bars.

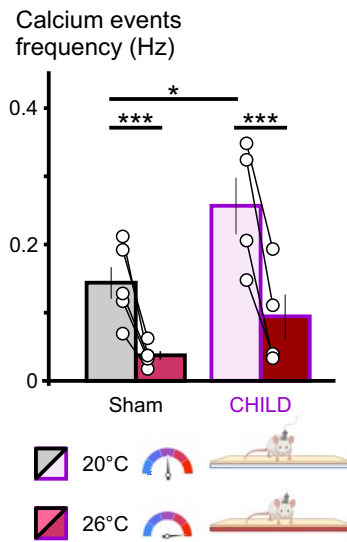












576 Methods.

577 **Animals.** CD1 mice were initially obtained from Janvier (Le Genest-Saint-Isle, France) and
578 subsequently bred in-house. Animals were kept in groups, in standard housing conditions
579 (21°C, 55% humidity, 12h light-dark cycle) and had access to *ad libitum* food and water. At
580 postnatal day 17, 9 males were randomly assigned to a sham (n=5) or juvenile mTBI (CHILD,
581 n=4) group. Forty-one to forty-six days later animals from both groups were stereotaxically
582 transfected and implanted with a miniscope lens (Inscopix GRIN lens, Palo Alto, CA). A
583 month later, and every 3 months after the CHILD/sham procedure and up to a year
584 afterwards, animals were tested in behavioral challenges while calcium imaging recordings
585 were performed (Figure 1). All animal procedures were carried out in accordance with the
586 University of Bordeaux animal care committee regulations, French laws governing laboratory
587 animal use (authorization #29324-2021012118549817 v3), the European Council directives
588 (86/609/EEC) and the ARRIVE guidelines.

589 **Closed-Head Injury with Long-term Disorders (CHILD) model.** Concussions were
590 performed at postnatal day 17 as previously described using the CHILD model^{18,28}. Briefly,
591 under isoflurane anesthesia (2.5%, 1.5 l/min) male mice were impacted over the left
592 somatosensory cortex using an electromagnetic impactor (Leica Impact One Stereotaxic
593 impactor, Leica Biosystems, Richmond, IL, USA) with a 3 mm round tip (3 m/s, 3 mm depth
594 and 100 ms dwell time). For the sham procedure, animals underwent the same procedure
595 but were moved away from the impactor before impact. All mice were allowed to recover in
596 an individual cage before being returned to their home cage.

597 **Surgical procedure.** Viral transfection and miniscope implantation were performed at
598 postnatal days 58 to 63 on CHILD and sham mice. Forty-five minutes before the procedure,
599 mice received a subcutaneous injection of buprenorphine (0.05 mg/kg) and saline for
600 hydration. Under isoflurane (Centravet, Mazères, France) anesthesia (induction at 4%, then
601 maintained at 1 to 2 %), mice were then locally shaved and disinfected (betadine, Centravet,
602 Mazères, France). After securing the animal's head into a stereotaxic frame, a subcutaneous
603 injection of lidocaine was performed and the scalp was removed. Two skull screws were
604 secured on the right part of the skull while a 1x1.4 mm cranial window was drilled over the
605 left somatosensory cortex (AP: -1, ML: -1.8). Viral injections (INSCOPIX ready-to image
606 AAV1.camk2a.GCaMP6f.WPRE.bGHpA) were performed using a Hamilton syringe mounted
607 on a syringe nanoliter infusion system (legato 130, KD scientific, Holliston USA, 250nl/site at
608 25 nl/min) at the same location (DV: -0.4 and -0.6). After 10 min to allow for viral diffusion, a
609 GRIN lens (Inscopix) was lowered into position (AP: -1, ML: -1.8, DV: -1.2). Brain tissue was
610 then covered with a thin layer of kwik sil (WPI, France) and the grin lens position secured
611 with C&B-Metabond (Parkell, Edgewood, NY, USA) and the skull screws. This was then
612 embedded into an additional layer of dental cement. Mice recovered for at least 3 weeks to
613 allow GCaMP6f expression.

614 **Behavioral evaluation.** All behavioral evaluations were performed together with calcium
615 imaging recording. Therefore, each behavioral session was preceded by the mounting of the
616 miniscope onto the GRIN lens followed by a 5-minute habituation period. All sessions were
617 performed during animal's day-cycle (around 3 hours after light), in a quiet environment and
618 under controlled lighting. Each apparatus was cleaned with 75% ethanol before testing of
619 each animal to prevent potential bias due to olfactory cues.

620 **Behavioral evaluation – Elevated plus maze.** The homemade apparatus was made of a
621 black polymer and consisted of 4 arms of 35 cm length and 6 cm wide, with 2 opposite arms
622 with 18-cm-high walls (typically 15 lux) while the 2 other arms were opened to the depth
623 (typically 60 lux) and a central square of 6x6 cm. The apparatus was elevated to a height of

624 60 cm above a platform, itself 60 cm above ground. The animal was positioned at the start of
625 each test on an open arm, facing towards the edge, and was allowed to explore for 5
626 minutes. The time and distance spent into the open and closed arms, as well as in the
627 central square were monitored and analyzed with Any-Maze (version 7.3, Stoelting Europe,
628 Dublin Ireland). Head entrances in each part of the apparatus were also timed for
629 synchronization with calcium imaging recordings. This test was performed 6, 9 and 12
630 months after the injury.

631 **Behavioral evaluation – Novel object recognition test.** The apparatus consisted of a
632 custom-made arena (typically 60 lux) with a uniform, smooth black floor (45 x 45 cm) and
633 walls (35 cm high). On day one, mice were habituated to the empty open field during 5
634 minutes. On days 2 to 4, two standard 50 ml transparent culture flasks (4 cm wide, 11 cm
635 tall, and 2.5 cm wide) with a blue cap filled with red-stained sand identical were positioned in
636 opposite corners, 15 cm away from two consecutive walls. Animals were allowed to explore
637 the arena and the objects for 5 minutes per session. On day 5, one of the objects was
638 switched to a novel object consisting of 2 large white building blocks (8 cm wide, 2 cm tall,
639 and 2.5 cm width) with a smaller light blue building block (6 cm wide, 2cm tall and 2.5 cm
640 width) in between, and mice were allowed to explore for 5 minutes. Tracking was performed
641 using Any-Maze. An area of 5 cm around each object was defined as the area of interest.
642 The discrimination index was calculated as the percentage of time spent exploring the target
643 divided by total time spent exploring both targets.

644 **Behavioral evaluation – Beam walk.** For this test, mice had to cross a 30 cm custom-made
645 beams of 3, 2 or 1 cm wide (2 trials each) transparent plastic. The starting point was highly
646 illuminated (120 lux) while the goal area was dim (15 lux). Each trial was videotaped for
647 offline recording, focusing on the right side of the animal. Time to cross the beam was
648 manually scored and errors of the rear right paw were precisely timestamped.

649 **Behavioral evaluation – Rotarod.** This test was designed to focus on sensory integration
650 rather than motor learning. For this purpose, initial phase of the test was performed at the
651 fixed speed of 4 rotations per minute (RPM) and consisted of leaving the animal on the rod
652 for a minute total, replacing the animal on the rod in case of a fall. Once the 1 min criteria
653 reached, the animal was allowed to rest for an extra minute. The animal was then replaced
654 on the rod at a starting speed of 4 RPM. The speed was then immediately linearly increased
655 to reach 40 RPM after 2 min. Time and speed at fall were scored, and the session was
656 videotaped.

657 **Temperature assay – Hot plate.** For this test, the animal was allowed to rest on a plate at
658 room temperature (20°C) for 30 seconds. Mice were then positioned on a vivarium-type
659 heating pad (26°C) for another 30 seconds. The session was videotaped for calcium imaging
660 synchronization.

661 **Pharmacology.** 12 months post-injury, the effects of endocannabinoid degradation blockade
662 inhibition were tested. For this purpose, a first 5 min home cage session was performed for
663 baseline. The animal was then injected with JZL¹⁸⁴ (4-nitrophenyl 4-[bis(2H-1,3-benzodioxol-
664 5-yl)(hydroxy)methyl]piperidine-1-carboxylate, 18 mg/kg, Sigma-Aldrich, St. Louis, MO, USA,
665 dissolved in 10 % DMSO, 2% Tween 80 in saline) and subsequently positioned back into the
666 cage. Thirty minutes later, calcium imaging recording was resumed for 5 minutes to evaluate
667 the effect of the drug in absence of significant sensory stimulation. Finally, the animal was
668 tested in the elevated plus maze, as described above.

669 **Calcium imaging sessions.** Recording sessions were performed while the animal's
670 behavior was also videotaped. Synchrony of the videos was ensured with a LED indicating

671 recording of calcium imaging. Calcium imaging videos (1280 x 800 pixels) were sampled at
672 20kHz with an exposure time of 50 ms and a gain of 2 using a Nvista3 miniscope system
673 (Inscopix, Palo Alto, CA). Once the microscope was connected to the GRIN lens baseplate,
674 the focal plan of the session was set in order to recover the focal plan determined on the very
675 first imaging session, when possible (the first session aimed at identifying the best focal
676 plane with a maximum number of active cells). Typically, this step lasted around 20 seconds.

677 **Ex vivo analysis.** For *post-mortem* analysis, one week after the last behavioral assay, mice
678 were deeply anesthetized (100 mg/kg Ketamine/ 20 mg/kg xylazine) and fixed with an
679 intracardiac perfusion of a 4% PFA solution (in PBS), decapitated and the head was post-
680 fixed for 2 days in a 4% PFA solution (in PBS). After washing the heads with PBS-azide
681 (0.1%), miniscope lenses were carefully removed from the skull and the heads were stored
682 at 4°C in PBS-azide.

683 **Ex vivo analysis – Magnetic resonance imaging (MRI).** Ex vivo MRI was performed in a
684 7T scanner (Bruker BioSpin, Ettlingen, Germany) on whole brain samples from 10 rodents.
685 The brain was placed into a 50ml Falcon tube, secured to minimize movement and immersed
686 in Fluorinert solution (Synquest Laboratories) to minimize susceptibility artefacts. Imaging
687 parameters were as follows: multi echo T2-weighted imaging (T2WI):TR/TE (6000/6.61 ms),
688 FOV (20 x 20 mm), matrix (128 x 128), slice thickness (0.468 mm), and 25 echoes; diffusion
689 tensor imaging (DTI)—TR/TE (1000/38 ms), slice thickness (0.156 mm), 30 diffusion gradient
690 directions (b = 2000 mT/m), FOV (20 x 15 x 10 mm), with a matrix size of 128 x 96 x 48.

691 **Ex vivo analysis – Immunohistochemistry.** Once scanned with MRI, brains were extracted
692 from the skull and coronally sliced using a vibratome (Leica VS 1000, Leica Biosystems,
693 Deer Park, IL). The fifty micron-thick slices were stored in PBS-azide (0.1%). On the day of
694 staining, slices were washed in PBS and incubated in blocking solution (1% BSA, 0.3%
695 Triton X-100 in PBS) for 10 min. Slices were then incubated overnight at 4°C in blocking
696 solution containing a rabbit anti-Parvalbumin (PV) antibody (1:400, cat # PA1933, Thermo
697 Fisher Scientific, Waltham, MA). Slices were then washed and incubated blocking solution
698 containing a secondary antibody donkey anti-rabbit Alexa⁵⁶⁸ diluted to 1:1000 (Abcam,
699 Cambridge, MA) for 90 minutes. After several washes, slices were finally mounted onto glass
700 slides and cover-slipped using Vectashield (Vector Laboratories, Burlingame, CA) with DAPI
701 (1/10000, Thermo Fisher Scientific). Slides were then kept at 4°C until imaging.
702 Fluorescence image acquisitions were performed using a DS-Qi1Mc camera (Nikon Europe,
703 Stroombaan, Netherlands) mounted onto an epifluorescence Nikon eclipse 90i microscope
704 (Nikon Europe) and using the NIS Element software (Nikon, version 4.30.02). LED
705 illumination was provided by a pE-300^{white} CoolLED light source (coolLED, Handover, UK).

706 **Data analysis – MRI processing.** Both T2WI and DTI scans were skull stripped with the
707 segmentation tool from the ITK-SNAP software (version 3.8.0, RRID:SCR_002010)⁷¹. DTI
708 images underwent denoising using the Adaptive Optimized Non-Local Means (AONLM)
709 filter⁷², followed by eddy current and bias field correction⁷³. Tractography was then
710 undertaken by using the somatosensory cortex (SSC) and ventral posterior thalamic nuclei
711 (VPLM) regions from the Australian Mouse Brain Mapping Consortium (AMBMC) atlas^{74,75}.
712 These regions were non-linearly registered to each animal's averaged DTI b0s using
713 Advanced Normalization Tools (ANTs, RRID:SCR_004757). The diffusion data were
714 reconstructed using generalized q-sampling imaging⁷⁶ with a diffusion sampling length ratio
715 of 0.75. The VPLM was seeded and tracts to the SSC were reconstructed with a tracking
716 threshold of 0.016, an angular threshold of 65, and a step size of 0.2. In this study, we
717 tracked projections from the VPLM to the SSC through the caudate putamen, with reference
718 to mouse viral tracing data from the Allen Brain Institute (<http://mouse.brain-map.org/>,
719 Experiment 100141223). Animals whose tracts did not match the anticipated structure were

720 excluded from tractography analysis, leaving us with 3 sham and 3 TBI subjects. Diffusion
721 tensor metrics fractional anisotropy (FA), axial diffusivity (AxD), mean diffusivity (MD), and
722 radial diffusivity (RD) were extracted from the tract⁷⁷. Additional shape metrics used to
723 characterize additional structural properties, including span, curl, volume, and diameter of the
724 tract were also extracted⁷⁸.

725 **Data analysis – Behavior.** For the elevated plus maze and the novel object recognition test,
726 Any-Maze was used to define the behavior of the animals. The time spent and timing of
727 entries in user-defined areas were collected to define neuronal activity in each compartment.
728 For the beam walk and rotarod tests, the data was manually scored. For all these tests, data
729 was fed into an excel template or python script in order to sort calcium events according to
730 the behavior.

731 **Data analysis – calcium imaging.** First steps of the analysis were performed using Inscopix
732 Data Processing Software (version 1.6.0.3225, Inscopix). For the novel object test and
733 pharmacology experiments videos were concatenated in order to follow neuronal activity of
734 each cell precisely. Briefly, processing included a spatial down sampling (factor 2) and
735 filtering (low cut-off 0.05 pixel⁻¹, high cut-off 0.5 pixel⁻¹). Motion correction was then applied
736 and the $\Delta F/F$ movie (mean frame as reference) was created. A maximum image projection
737 was then created and used to manually draw ROIs. These ROIs were then used to extract
738 fluorescence variations across the $\Delta F/F$ movie. These traces were then deconvoluted (model
739 order 1, Spike SNR threshold 3) and calcium-related events detected (event threshold factor
740 4, event smallest decay time 200 ms). Deconvoluted traces and events parameters were
741 then fed into an excel template or python script for event sorting, traces reconstruction and z-
742 score calculation. For each time point, the z-score was defined as the $\Delta F/F$ value of that time
743 point minus the mean of $\Delta F/F$ values of the session divided by the standard deviation of $\Delta F/F$
744 values of the session and was calculated with a python script.

745 **Data analysis – classification algorithm.** 3 modalities were fed to a home-made
746 classification algorithm using data obtained in neutral condition (home cage, average
747 neuronal activity), amplitude of the network's response to the entry in the open arms of the
748 elevated plus maze and number of entries of the animal in those arms. Data was converted
749 into numerical arrays for TensorFlow compatibility. A neural network model was constructed
750 using TensorFlow's Keras API, comprising multiple densely connected layers and an output
751 layer using the softmax activation function for multi-class classification. The model was
752 compiled with the Adam optimizer, categorical cross-entropy loss function, and accuracy as
753 the evaluation metric. The model was trained on the dataset comprising data collected at 6
754 and 9 MPI on all animals. To avoid overfitting of the data, the model was trained on a
755 maximum of 2000 epochs with an early stopping callback function set at 500 epochs as
756 failsafe. Hence, the algorithm reached a loss of 0.0589 with an accuracy of 1. The model's
757 performance was then evaluated on separate test datasets collected at 12 MPI, with JZL
758 injection and vehicle injection protocols using the evaluate method. Finally, predictions were
759 generated for both test datasets using the trained model.

760 **Data analysis – codes and statistics.** Behavior and calcium imaging were processed using
761 custom-made excel templates and python scripts, all available upon reasonable requests.
762 Data sets used in this study originated from 2 independent replicates and mice that
763 originated from 3 different litters were randomly assigned to the sham or CHILD group. All
764 values are presented as mean \pm SEM. For each statistical analysis normality and equality of
765 the variances were assessed. two-sided tests were used and a p value < 0.05 was
766 considered as significant. When needed, 2-way ANOVAs with repeated measurements and
767 *post hoc* Tukey tests were performed. All statistical tests on behavior tests were performed
768 on primary data (not normalized), and statistical tests on calcium imaging were performed on

769 event detection performed on deconvoluted $\Delta F/F$ traces. For detailed statistical analysis, see
770 the Supplementary table 1. Data are available upon request from the corresponding author.

771 References.

- 772 1. Giza, C. C. & Prins, M. L. Is being plastic fantastic? Mechanisms of altered plasticity after
773 developmental traumatic brain injury. *Dev Neurosci* **28**, 364–379 (2006).
- 774 2. McMahon, P. *et al.* Symptomatology and functional outcome in mild traumatic brain injury: results
775 from the prospective TRACK-TBI study. *J Neurotrauma* **31**, 26–33 (2014).
- 776 3. Ruff, R. Two decades of advances in understanding of mild traumatic brain injury. *J Head Trauma*
777 *Rehabil* **20**, 5–18 (2005).
- 778 4. Iverson, G. L. *et al.* Predictors of clinical recovery from concussion: a systematic review. *Br J*
779 *Sports Med* **51**, 941–948 (2017).
- 780 5. Zemek, R. *et al.* Clinical Risk Score for Persistent Postconcussion Symptoms Among Children With
781 Acute Concussion in the ED. *JAMA* **315**, 1014–1025 (2016).
- 782 6. Campbell, K. R. *et al.* Exploring persistent complaints of imbalance after mTBI: Oculomotor,
783 peripheral vestibular and central sensory integration function. *J Vestib Res* **31**, 519–530 (2021).
- 784 7. Ding, M.-C., Wang, Q., Lo, E. H. & Stanley, G. B. Cortical excitation and inhibition following focal
785 traumatic brain injury. *J Neurosci* **31**, 14085–14094 (2011).
- 786 8. Bonislawski, D. P., Schwarzbach, E. P. & Cohen, A. S. Brain injury impairs dentate gyrus inhibitory
787 efficacy. *Neurobiology of Disease* **25**, 163–169 (2007).
- 788 9. Lowenstein, D. H., Thomas, M. J., Smith, D. H. & McIntosh, T. K. Selective vulnerability of dentate
789 hilar neurons following traumatic brain injury: a potential mechanistic link between head trauma and
790 disorders of the hippocampus. *J Neurosci* **12**, 4846–4853 (1992).
- 791 10. Jacotte-Simancas, A. *et al.* Brain Injury Effects on Neuronal Activation and Synaptic
792 Transmission in the Basolateral Amygdala of Adult Male and Female Wistar Rats. *J Neurotrauma*
793 **39**, 544–559 (2022).
- 794 11. Fucich, E. A. *et al.* Endocannabinoid degradation inhibitors ameliorate neuronal and synaptic
795 alterations following traumatic brain injury. *Journal of Neurophysiology* **123**, 707–717 (2020).
- 796 12. Mayeux, J. P., Teng, S. X., Katz, P. S., Gilpin, N. W. & Molina, P. E. Traumatic brain injury
797 induces neuroinflammation and neuronal degeneration that is associated with escalated alcohol
798 self-administration in rats. *Behav Brain Res* **279**, 22–30 (2015).
- 799 13. Akasu, T., Muraoka, N. & Hasuo, H. Hyperexcitability of hippocampal CA1 neurons after fluid
800 percussion injury of the rat cerebral cortex. *Neurosci Lett* **329**, 305–308 (2002).
- 801 14. Yang, L. *et al.* Spontaneous epileptiform activity in rat neocortex after controlled cortical
802 impact injury. *J Neurotrauma* **27**, 1541–1548 (2010).
- 803 15. Ai, J. & Baker, A. Presynaptic hyperexcitability at cerebellar synapses in traumatic injury rat.
804 *Neuroscience Letters* **332**, 155–158 (2002).
- 805 16. Nichols, J., Perez, R., Wu, C., Adelson, P. D. & Anderson, T. Traumatic brain injury induces
806 rapid enhancement of cortical excitability in juvenile rats. *CNS Neurosci Ther* **21**, 193–203 (2015).
- 807 17. Khodaie, B. *et al.* Structural and functional effects of social isolation on the hippocampus of
808 rats with traumatic brain injury. *Behav Brain Res* **278**, 55–65 (2015).
- 809 18. Obenaus, A. *et al.* A single mild juvenile TBI in male mice leads to regional brain tissue
810 abnormalities at 12 months of age that correlate with cognitive impairment at the middle age. *Acta*
811 *Neuropathol Commun* **11**, 32 (2023).
- 812 19. Ohno-Shosaku, T. & Kano, M. Endocannabinoid-mediated retrograde modulation of synaptic
813 transmission. *Current Opinion in Neurobiology* **29**, 1–8 (2014).
- 814 20. Heifets, B. D. & Castillo, P. E. Endocannabinoid signaling and long-term synaptic plasticity.
815 *Annu Rev Physiol* **71**, 283–306 (2009).
- 816 21. Dubois, C. J., Fawcett-Patel, J., Katzman, P. A. & Liu, S. J. Inhibitory neurotransmission
817 drives endocannabinoid degradation to promote memory consolidation. *Nat Commun* **11**, 6407
818 (2020).
- 819 22. Marsicano, G. & Lutz, B. Neuromodulatory functions of the endocannabinoid system. *J*
820 *Endocrinol Invest* **29**, 27–46 (2006).
- 821 23. Walter, L. & Stella, N. Cannabinoids and neuroinflammation. *Br J Pharmacol* **141**, 775–785
822 (2004).
- 823 24. Giacobbe, J., Marrocu, A., Di Benedetto, M. G., Pariente, C. M. & Borsini, A. A systematic,
824 integrative review of the effects of the endocannabinoid system on inflammation and neurogenesis
825 in animal models of affective disorders. *Brain Behav Immun* **93**, 353–367 (2021).
- 826 25. Hashimoto-dani, Y. *et al.* Acute inhibition of diacylglycerol lipase blocks endocannabinoid-
827 mediated retrograde signalling: evidence for on-demand biosynthesis of 2-arachidonoylglycerol.
828 *The Journal of physiology* **591**, 4765–4776 (2013).
- 829 26. Xu, J.-Y. & Chen, C. Endocannabinoids in synaptic plasticity and neuroprotection.
830 *Neuroscientist* **21**, 152–168 (2015).

- 831 27. Chen, C. Inhibiting degradation of 2-arachidonoylglycerol as a therapeutic strategy for
832 neurodegenerative diseases. *Pharmacol Ther* **244**, 108394 (2023).
- 833 28. Rodriguez-Grande, B. *et al.* Gliovascular changes precede white matter damage and long-
834 term disorders in juvenile mild closed head injury. *Glia* **66**, 1663–1677 (2018).
- 835 29. Leyba, K. *et al.* Neurovascular hypoxia after mild traumatic brain injury in juvenile mice
836 correlates with heart-brain dysfunctions in adulthood. *Acta Physiol (Oxf)* **238**, e13933 (2023).
- 837 30. Viaene, A. N., Petrof, I. & Sherman, S. M. Synaptic properties of thalamic input to layers 2/3
838 and 4 of primary somatosensory and auditory cortices. *J Neurophysiol* **105**, 279–292 (2011).
- 839 31. Ndode-Ekane, X. E., Puigferrat Pérez, M. D. M., Di Sapia, R., Lapinlampi, N. & Pitkänen, A.
840 Reorganization of Thalamic Inputs to Lesioned Cortex Following Experimental Traumatic Brain
841 Injury. *Int J Mol Sci* **22**, 6329 (2021).
- 842 32. Fidan, E. *et al.* Repetitive Mild Traumatic Brain Injury in the Developing Brain: Effects on
843 Long-Term Functional Outcome and Neuropathology. *J Neurotrauma* **33**, 641–651 (2016).
- 844 33. Kasahara, M. *et al.* Altered functional connectivity in the motor network after traumatic brain
845 injury. *Neurology* **75**, 168–176 (2010).
- 846 34. Zhu, D., Gao, F. & Chen, C. Endocannabinoid Metabolism and Traumatic Brain Injury. *Cells*
847 **10**, 2979 (2021).
- 848 35. Mechoulam, R., Spatz, M. & Shohami, E. Endocannabinoids and neuroprotection. *Sci STKE*
849 **2002**, re5 (2002).
- 850 36. Durieux, L. J. A., Gilissen, S. R. J. & Arckens, L. Endocannabinoids and cortical plasticity:
851 CB1R as a possible regulator of the excitation/inhibition balance in health and disease. *Eur J*
852 *Neurosci* **55**, 971–988 (2022).
- 853 37. Baraibar, A. M. *et al.* Spatial organization of neuron-astrocyte interactions in the
854 somatosensory cortex. *Cereb Cortex* **33**, 4498–4511 (2023).
- 855 38. Marinelli, S. *et al.* The endocannabinoid 2-arachidonoylglycerol is responsible for the slow
856 self-inhibition in neocortical interneurons. *J Neurosci* **28**, 13532–13541 (2008).
- 857 39. Fortin, D. A. & Levine, E. S. Differential effects of endocannabinoids on glutamatergic and
858 GABAergic inputs to layer 5 pyramidal neurons. *Cereb Cortex* **17**, 163–174 (2007).
- 859 40. Long, J. Z., Nomura, D. K. & Cravatt, B. F. Characterization of Monoacylglycerol Lipase
860 Inhibition Reveals Differences in Central and Peripheral Endocannabinoid Metabolism. *Chemistry &*
861 *Biology* **16**, 744–753 (2009).
- 862 41. Gulati, S., Cao, V. Y. & Otte, S. Multi-layer Cortical Ca²⁺ Imaging in Freely Moving Mice with
863 Prism Probes and Miniaturized Fluorescence Microscopy. *J Vis Exp* 55579 (2017)
864 doi:10.3791/55579.
- 865 42. Huh, J. W. & Raghupathi, R. Therapeutic strategies to target acute and long-term sequelae of
866 pediatric traumatic brain injury. *Neuropharmacology* **145**, 153–159 (2019).
- 867 43. Serpa, R. O. *et al.* Pathophysiology of Pediatric Traumatic Brain Injury. *Front Neurol* **12**,
868 696510 (2021).
- 869 44. Katz, P. S. *et al.* Endocannabinoid Degradation Inhibition Improves Neurobehavioral Function,
870 Blood–Brain Barrier Integrity, and Neuroinflammation following Mild Traumatic Brain Injury. *Journal*
871 *of Neurotrauma* **32**, 297–306 (2015).
- 872 45. Hu, M. *et al.* Enhancing endocannabinoid signalling in astrocytes promotes recovery from
873 traumatic brain injury. *Brain* **145**, 179–193 (2022).
- 874 46. Papa, A. *et al.* Polypharmacological Approaches for CNS Diseases: Focus on
875 Endocannabinoid Degradation Inhibition. *Cells* **11**, 471 (2022).
- 876 47. Schurman, L. D. & Lichtman, A. H. Endocannabinoids: A Promising Impact for Traumatic
877 Brain Injury. *Front Pharmacol* **8**, 69 (2017).
- 878 48. Shohami, E., Cohen-Yeshurun, A., Magid, L., Algali, M. & Mechoulam, R. Endocannabinoids
879 and traumatic brain injury. *Br J Pharmacol* **163**, 1402–1410 (2011).
- 880 49. Kolb, B., Saber, H., Fadel, H. & Rajah, G. The endocannabinoid system and stroke: A focused
881 review. *Brain Circ* **5**, 1–7 (2019).
- 882 50. Basavarajappa, B. S., Shivakumar, M., Joshi, V. & Subbanna, S. Endocannabinoid system in
883 neurodegenerative disorders. *J Neurochem* **142**, 624–648 (2017).
- 884 51. Taylor, C. A., Bell, J. M., Breiding, M. J. & Xu, L. Traumatic Brain Injury–Related Emergency
885 Department Visits, Hospitalizations, and Deaths — United States, 2007 and 2013. *MMWR Surveill.*
886 *Summ.* **66**, 1–16 (2017).
- 887 52. Giza, C. C., Mink, R. B. & Madikians, A. Pediatric traumatic brain injury: not just little adults.
888 *Curr Opin Crit Care* **13**, 143–152 (2007).
- 889 53. Babikian, T. *et al.* The UCLA longitudinal study of neurocognitive outcomes following mild
890 pediatric traumatic brain injury. *J Int Neuropsychol Soc* **17**, 886–895 (2011).

- 891 54. Ichkova, A. *et al.* Early cerebrovascular and long-term neurological modifications ensue
892 following juvenile mild traumatic brain injury in male mice. *Neurobiol Dis* **141**, 104952 (2020).
- 893 55. Prins, M., Greco, G., Alexander, A. & Giza, C. C. The pathophysiology of traumatic brain injury
894 at a glance. *Disease models & mechanisms* **6**, (2013).
- 895 56. Cai, H. *et al.* Amygdalo-nigral circuit mediates stress-induced vulnerability to the parkinsonian
896 toxin MPTP. *CNS Neuroscience & Therapeutics* **n/a**.
- 897 57. Torre-Muruzabal, T. *et al.* Chronic nigral neuromodulation aggravates behavioral deficits and
898 synaptic changes in an α -synuclein based rat model for Parkinson's disease. *Acta Neuropathol*
899 *Commun* **7**, 160 (2019).
- 900 58. Ayaz, A. *et al.* Layer-specific integration of locomotion and sensory information in mouse
901 barrel cortex. *Nat Commun* **10**, 2585 (2019).
- 902 59. Bernardi, N. F., Darainy, M. & Ostry, D. J. Somatosensory Contribution to the Initial Stages of
903 Human Motor Learning. *J. Neurosci.* **35**, 14316–14326 (2015).
- 904 60. Mirdamadi, J. L. & Block, H. J. Somatosensory changes associated with motor skill learning. *J*
905 *Neurophysiol* **123**, 1052–1062 (2020).
- 906 61. Yu, Y. *et al.* Layer-specific activation in human primary somatosensory cortex during tactile
907 temporal prediction error processing. *Neuroimage* **248**, 118867 (2022).
- 908 62. Chang, C.-W. *et al.* A Cortico-Cortical Pathway Targets Inhibitory Interneurons and Modulates
909 Paw Movement during Locomotion in Mice. *J Neurosci* **42**, 44–57 (2022).
- 910 63. Vestergaard, M., Carta, M., Güney, G. & Poulet, J. F. A. The cellular coding of temperature in
911 the mammalian cortex. *Nature* **614**, 725–731 (2023).
- 912 64. Chen, X.-J., Liu, Y.-H., Xu, N.-L. & Sun, Y.-G. Multiplexed Representation of Itch and
913 Mechanical and Thermal Sensation in the Primary Somatosensory Cortex. *J Neurosci* **41**, 10330–
914 10340 (2021).
- 915 65. Hellon, R. F., Misra, N. K. & Provins, K. A. Neurones in the somatosensory cortex of the rat
916 responding to scrotal skin temperature changes. *J Physiol* **232**, 401–411 (1973).
- 917 66. Kreitzer, A. C., Carter, A. G. & Regehr, W. G. Inhibition of interneuron firing extends the
918 spread of endocannabinoid signaling in the cerebellum. *Neuron* **34**, 787–796 (2002).
- 919 67. Carzoli, K. L., Kogias, G., Fawcett-Patel, J. & Liu, S. J. Cerebellar interneurons control fear
920 memory consolidation via learning-induced HCN plasticity. *Cell Rep* **42**, 113057 (2023).
- 921 68. Soti, M. *et al.* Probable role of the hyperpolarization-activated current in the dual effects of
922 CB1R antagonism on behaviors in a Parkinsonism mouse model. *Brain Res Bull* **191**, 78–92
923 (2022).
- 924 69. Maroso, M. *et al.* Cannabinoid Control of Learning and Memory through HCN Channels.
925 *Neuron* **89**, 1059–1073 (2016).
- 926 70. Hashimoto-dani, Y., Ohno-Shosaku, T. & Kano, M. Endocannabinoids and synaptic function in
927 the CNS. *Neuroscientist* **13**, 127–137 (2007).
- 928 71. Yushkevich, P. A. *et al.* User-guided 3D active contour segmentation of anatomical structures:
929 significantly improved efficiency and reliability. *Neuroimage* **31**, 1116–1128 (2006).
- 930 72. Manjón, J. V., Coupé, P., Martí-Bonmatí, L., Collins, D. L. & Robles, M. Adaptive non-local
931 means denoising of MR images with spatially varying noise levels. *J Magn Reson Imaging* **31**, 192–
932 203 (2010).
- 933 73. Tustison, N. J. *et al.* N4ITK: improved N3 bias correction. *IEEE Trans Med Imaging* **29**, 1310–
934 1320 (2010).
- 935 74. Ullmann, J. F. P., Watson, C., Janke, A. L., Kurniawan, N. D. & Reutens, D. C. A
936 segmentation protocol and MRI atlas of the C57BL/6J mouse neocortex. *Neuroimage* **78**, 196–203
937 (2013).
- 938 75. Richards, K. *et al.* Segmentation of the mouse hippocampal formation in magnetic resonance
939 images. *Neuroimage* **58**, 732–740 (2011).
- 940 76. Yeh, F.-C., Wedeen, V. J. & Tseng, W.-Y. I. Generalized q-sampling imaging. *IEEE Trans*
941 *Med Imaging* **29**, 1626–1635 (2010).
- 942 77. Obenaus, A. & Jacobs, R. E. Magnetic resonance imaging of functional anatomy: use for
943 small animal epilepsy models. *Epilepsia* **48 Suppl 4**, 11–17 (2007).
- 944 78. Yeh, F.-C. Shape analysis of the human association pathways. *Neuroimage* **223**, 117329
945 (2020).
- 946